

Interaction Replica: Tracking human–object interaction and scene changes from human motion

Vladimir Guzov^{1,2} Julian Chibane^{1,2} Riccardo Marin¹ Torsten Sattler³ Gerard Pons-Moll^{1,2}

¹University of Tübingen, Germany, ²Max Planck Institute for Informatics, Saarland Informatics Campus, Germany

³CIIRC, Czech Technical University in Prague, Czech Republic

{vladimir.guzov,riccardo.marin,gerard.pons-moll}@uni-tuebingen.de jchibane@mpi-inf.mpg.de torsten.sattler@cvut.cz

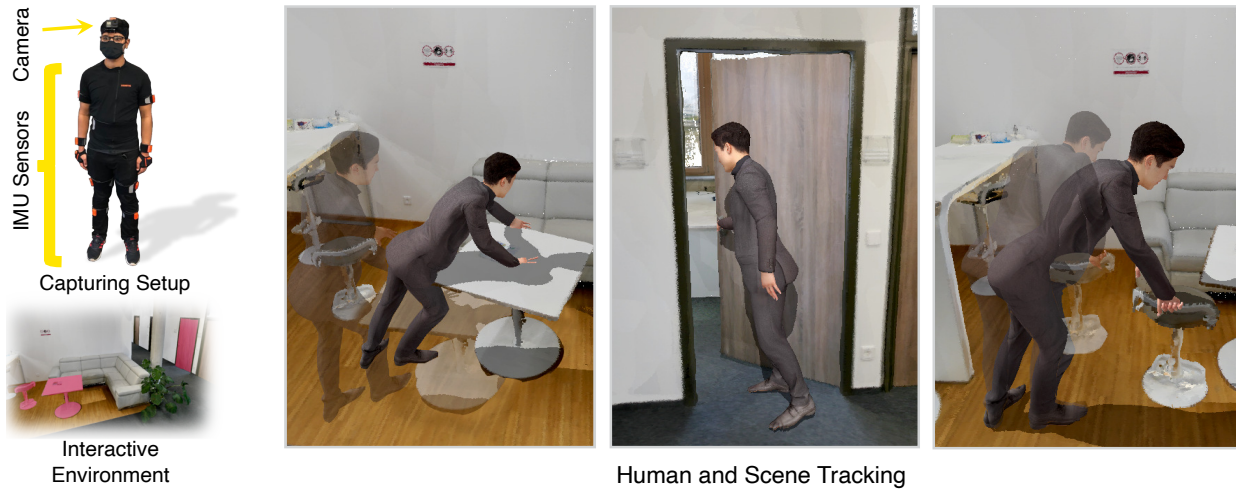


Figure 1: **Interaction Replica (iReplica)**. The inputs to our method are a motion sequence of a subject captured from wearable sensors and an interactive virtual environment (left). Using the wearable sensors, we localize and track the human and an object within the scene, creating a digital replica of the interactions (right).

Abstract

Humans naturally change their environment through interactions, e.g., by opening doors or moving furniture. To reproduce such interactions in virtual spaces (e.g., metaverse), we need to capture and model them, including changes in the scene geometry, ideally from egocentric input alone (head camera and body-worn inertial sensors). While the head camera can be used to localize the person in the scene, estimating dynamic object pose is much more challenging. As the object is often not visible from the head camera (e.g., a human not looking at a chair while sitting down), we can not rely on visual object pose estimation. Instead, our key observation is that human motion tells us a lot about scene changes. Motivated by this, we present iReplica, the first human–object interaction reasoning method which can track objects and scene changes based solely on human motion. iReplica is an essential first step towards advanced AR/VR applications in immersive virtual universes and can provide human-centric training data to teach machines to interact with their surroundings. Our code, data and model will be available on our project page at <http://virtualhumans.mpi-inf.mpg.de/ireplica/>.

1. Introduction

Current augmented and virtual reality (AR/VR) applications show promising potential: interesting applications include collaborative developments, virtual meeting rooms, and personal assistants that help users navigate the world. However, the current AR/VR experience is restricted to the virtual world. For an immersive experience, the device must integrate real-world information and blend physical and digital worlds. For example, consider a person showing you a skill remotely while moving physical objects, changing rooms and opening different doors in a building. On your AR/VR device, you should be able to see the full interaction, including the person and the scene changes.

Capturing such interactions across multiple rooms or in large spaces is not possible with external points of view, as ensuring complete coverage would require an unreasonable number of cameras: buying, mounting and calibrating them without any blind spots in tens of rooms is impractical. We foresee an increasing demand for AR/VR applications where users can move objects and interact freely in large environments. This calls for tracking solutions based solely on wearable sensors. Since most 3D human estimation methods rely on external cameras [26, 25, 42, 15, 21, 30, 71, 36],



Figure 2: **Visual occlusions.** During the interaction the head-mounted camera might only observe a part of the object with indistinctive features *e.g.*, texturless black sofa or a small piece of the table, which makes it impossible to localize the object from RGB.

few works have focused on such large-scene scenarios. One exception is HPS [16], which positions the person in the scene via head camera localization, while estimating the human motion from IMUs. However, HPS cannot track scene changes. As our experiments demonstrate, object pose cannot be reliably tracked from the head camera, as users often interact with objects without looking at them, and even when they do, the image is often blurry, suffers from heavy occlusion and lacks distinctive features (*cf.* Fig. 2).

How can we then track human motion and scene changes in large scenes from only wearable sensors? In this paper, we introduce *Interaction Replica (iReplica)*, the first method to address this unexplored challenge. The input to our method is an interactive environment (IE), consisting of a *static* 3D scan where interacting objects are segmented, and their classes and degrees of freedom are known. Such input can be obtained by pre-scanning the scene with LiDAR and segmenting objects before the interaction. From the IMUs and a head-mounted camera worn by the user (Fig. 1), iReplica creates a digital replica of the interaction (Fig. 3) by localizing the person within the 3D scene, detecting contacts, and inferring object pose trajectory. Since visual object localization is unreliable, our key contribution is a method to infer 3D object motion from human motion alone. This requires 1) automatically detecting contacts from the human pose alone, 2) correcting the human trajectory to satisfy the physical contact, and 3) inferring the 3D object pose trajectory coherent with the human motion. Our key finding is that human motion alone tells us a lot about contacts and the object pose, allowing us to capture interaction without suffering from the aforementioned visual object localization problems.

To train and evaluate our method on the new problems of inferring contact from the human pose and predicting object trajectories, we use two captured datasets: the Human-contact (H-contact) dataset consisting 3D human poses captured with IMUs for 30 minutes, along with manually labelled contact times for a total of 108k annotated frames, and the Egocentric Human-Object Interactions (EgoHOI) dataset including the 3D human motion, the 3D scene as an interactive environment, and annotations of object pose at the beginning and end of interactions, for 54k frames of



Figure 3: **Digital replica** of the real scene made by iReplica. On the right – a photo of a real human-object interaction captured with external camera, on the left - reconstruction by iReplica.

interactions with 9 objects. EgoHOI includes challenging interactions where an external camera system cannot be deployed (*e.g.*, multiple objects, multiple rooms).

Our experiments demonstrate that iReplica can capture full interactions, including the human motion, its location within the 3D scene and the scene changes, all from wearable sensors alone. We demonstrate that our human-centric approach outperforms baselines which rely on camera-based contact detection or visual object localization. Our work is a significant first step towards embodied capture of human-scene interactions, which can open a wide range of immersive AR/VR applications, for example, controlling objects in interactive environments by interacting with real-world objects. We will release the method code, the evaluation protocol, the datasets, and the motion capture data to facilitate further research in this area.

2. Related Work

Human-object interaction. Most current methods to record human-object interactions use external cameras. Methods to capture the full body pose also use external cameras and mostly static scenes [18, 71, 36] or work with a single dynamic object without any scene context [69, 65, 62, 56, 19, 4]; similarly for human-scene and human-object interaction generation methods [55, 72, 17, 54]. RigidFusion [63] tracks objects using an external RGBD sensor. Some methods work with first-person view footage, however, they mostly study the upper body, *e.g.*, hand-object pose estimation [57, 31, 34, 13, 39], and are mostly limited to static cameras. Our method works with body-mounted sensors and a moving camera while capturing the full-body pose and object position simultaneously.

Embodied research. Body-mounted sensor setups are heavily used to solve various tasks: activity recognition methods [3, 14, 38, 9, 66, 44] use egocentric cameras looking at the body. However, they typically concentrate on capturing the upper body. Many full-body capturing methods [43, 64, 59] work with similar head-mounted setups, but as the cameras are pointed at the person wearing them

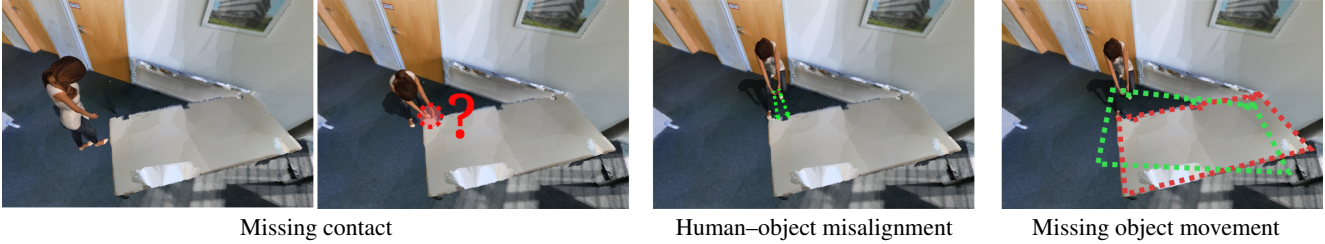


Figure 4: **Challenges.** In the image, we report a human–object interaction result from [16]. In red, we highlight missing or erroneous predictions; in green the ideal ones. Previous methods do not address contact prediction, human–object alignment, and object movements solely from wearable sensors. This motivates us to tackle these challenges.

rather than outwards, these methods do not consider the environment around the subject. Some methods work with an outwards-facing camera [23, 67, 68], however, they do not use any additional sensors to capture the body pose, and predict it using motion priors. This results in body poses far from the ground truth. [33] proposes action recognition and localization using a first-person perspective video but does not model scene change. [70] works with a head-mounted camera, but uses it to capture the pose of other subjects, essentially making it an external-camera method. Most related to our method, HPS [16] captures human motion using body-mounted IMUs and a head-mounted camera looking outwards to capture the location of the subject within a pre-built 3D scan of the environment. We extend HPS by not only tracking the human pose, but also an object the person interacts with. Whereas HPS is restricted to static environments and cannot model scene changes caused by human–object interactions, iReplica removes these restrictions.

Visual localization. Visual localization aim to estimate the pose of a camera in a known environment. Current state-of-the-art approaches are based on 2D–3D matches between pixels in the camera image and 3D scene points. These 2D–3D matches are either estimated based on local features [46, 48, 49, 20, 32, 37] or by regressing a 3D point coordinate for each pixel [52, 7, 6, 10, 12]¹. A recent line of works focuses on the robustness of localization algorithms [58, 61, 22, 12], *e.g.*, to illumination, weather, and seasonal changes, as well as to changes caused by human actions (rearranging furniture, *etc.*). These approaches assume that a large enough part of the scene remains static and is observed by the camera to facilitate pose estimation. The second assumption is violated in our scenario and we use IMU-based human pose tracking to bridge gaps where visual localization algorithms will most likely fail. As in [16], for the head-mounted camera localization we use a state-of-the-art localization pipeline [46, 47]. Note that our main contribution, *i.e.*, jointly reasoning about human and object pose, is not tied to any particular localization algorithm.

¹We refer the interested reader to [5] for a discussion and comparison of both types of approaches.

3. Method

Our work is the first to jointly track and localize humans together with scene changes resulting from interactions. Hence, here we formalise our main assumptions, input, and expected output.

Assumptions. We assume a given *interactive environment* (IE) consisting of a static 3D scan of the scene, along with a set of objects that the user can interact with. These objects are already segmented from the background scene, and their degrees of freedom are known, *e.g.*, we expect that a sofa can slide on the ground but not lift, and that a door rotates around a hinge. In practice, such an interactive environment can be acquired by scanning the scene with LiDAR and segmenting the objects before the interaction occurs.

Input. We require a set of body-mounted wearable IMUs (we use 17 sensors from XSens [41]) and video from a head-mounted camera. Wearable sensors allow us to capture interactions in unrestricted recording volumes across multiple rooms. As mentioned in the introduction, this would be much more challenging for external cameras capturing.

Output. iReplica outputs a virtual replica of the interaction, *i.e.*, coherent human and object motion in the scene.

Components. Our method has the following components:

1. **Predicting contact intervals:** Given the unreliable information from the camera, our idea is to estimate the start and the end of the contact relying only on the human pose information.
2. **Deforming the human trajectory to match the contact:** Human pose obtained from IMUs is prone to drifts, and contact prediction might not be completely accurate. Hence, to obtain realism, the human pose needs correction to match the detected contacts.
3. **Driving the object based on contacts:** We infer the object pose trajectory based on human contacts.

Overview. We provide an overview of the inference of our method for a single-object interaction; steps are depicted in Fig. 5. First, we obtain initial localization and pose estimation for the person relying on HPS [16]. At each in-

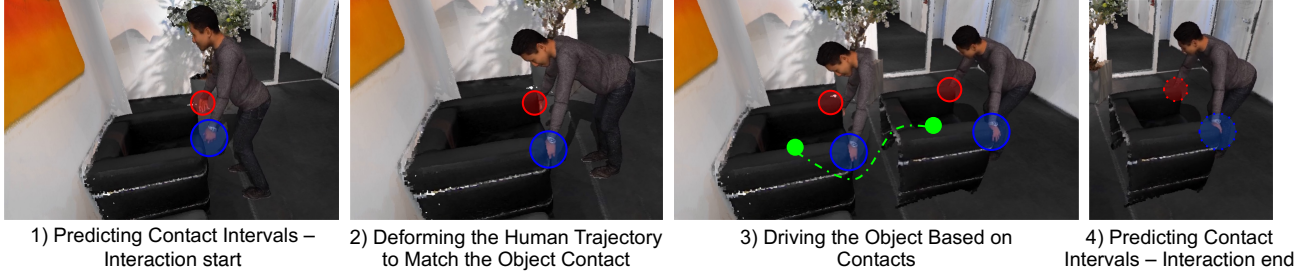


Figure 5: **Overview of iReplica.** iReplica tracks scene changes and creates visually plausible human–scene interactions in 4 steps. **1)** The start of interaction is predicted by a neural network. Predictions are performed as contact / no-contact classification of the subject’s hands (red and blue). **2)** The contacts are used to correct inaccurate localization of the human, snapping the human trajectory smoothly to the object. **3)** The motion of the contacted regions are used to infer the object trajectory (green). **4)** The network predicts the release of the interaction, which is essential to stop object dragging. The algorithm is detailed in our method section.

stant, our method considers only the human pose and predicts the probability of contact with an object. When the contact starts (1), we deform the human trajectory to match the object contact (2). Then, the object is attached to the human and driven in space according to its degrees of freedom (3). The object is released when our method infers from the human pose the end of the contact (4).

3.1. Predicting Contact Intervals

Input context. Existing datasets for human-object contact contain only a limited amount of samples per object type [4], or only hand-held objects [56]. In our context, the interaction involves large objects as elements of a complex scene. Hence, we collect and annotate a training dataset (Sec. 4.1) of $\sim 108k$ pose frames using IMUs. The size of our training set is comparable to the other human–object and human–scene interaction datasets (BEHAVE contains $\sim 15k$ frames, PROX $\sim 100k$). We will use our data to train a contact detection model based on human pose alone.

Transformer. To predict contact, we train a sequence-to-sequence Transformer [60] to map a sequence of 61 SMPL pose vectors to a per-hand contact probability for the central frame. Starting from the poses, we pass them to an MLP and append a positional encoding to the resulting features. Then, we process them with a Transformer to output a contact probability for each hand for the central (30th) frame. Using a sliding window approach, we obtain those probabilities for every frame (except for the first and last 30 frames of the sequence). The contact is considered active once the probability reaches a certain threshold. The architecture is depicted in Fig. 6. In ambiguous poses, the network may show an oscillatory behaviour, due to uncertainty during the start and the release of contact. To mitigate this, we post-process the predictions and fill the gaps between positive contacts shorter than 0.5 s to maintain the contact active. This value is found by experimenting with the validation set (see supplementary).

Contact intervals. Each group of consecutive frames with active contact is considered a *contact interval*. If the network predicts the end of the interaction only for one hand, while the other is still considered to be in contact, iReplica splits the contact interval into two consecutive interactions (a two-handed and a one-handed one). Similar cases (e.g., interchanging hands) are treated the same way.

3.2. Deforming the Human Trajectory to Match the Object Contact

Predicting the contact point. When the network predicts the start of the contact, we select the nearest object within a reasonable range (e.g., 50 cm). If no object is that close, the contact is ignored as a false positive. To improve robustness, we compute the *object contact* by averaging the 20 closest object points to the hand. We observed that such a simple choice is already effective.

Deforming the human trajectory. We deform the human trajectory to match the predicted object contact at the start. We observed that the human trajectory is reliable in general, while the global positioning from HPS is the main cause of error. Hence, we optimize for a single rotation to satisfy the initial object contact, while staying as close as possible to the original trajectory. If a sequence consists of multiple interactions, we apply the correction only once, to align the human with the first starting contact occurrence. We refer to the supplementary for more details.

3.3. Driving the Object Based on Contacts

After detecting the contact interval, we compute the object pose trajectory such that it is consistent with the human dynamics and contacts. We consider three cases, see Fig. 10.

A) Two-hand interaction for sliding objects. For interactions that involve both hands, we consider the vector that connects the right hand to the left one. The change in the vector angle is used to infer the rotation of the object, while

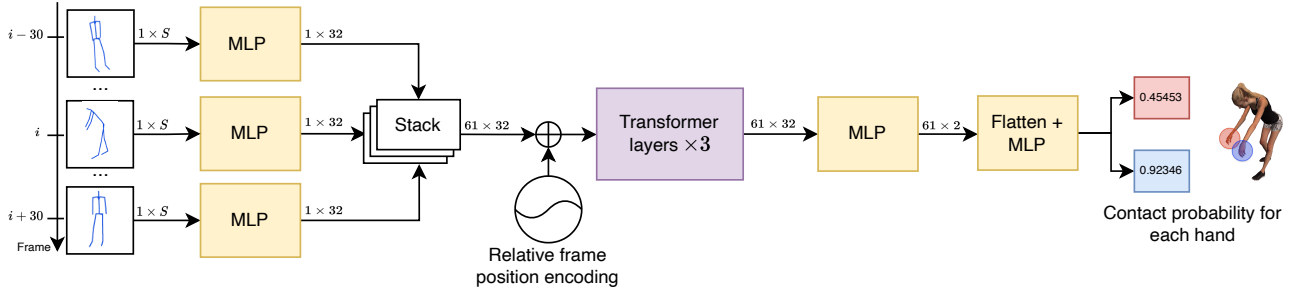


Figure 6: **Architecture of the contact prediction module.** Our Transformer-based architecture takes 61 frames $\{i - 30, \dots, i + 30\}$ of SMPL pose vectors of size $S = 69$ and predicts the contact probability for each hand for the middle frame i .

the translation of the right hand (left or right hand translation is arbitrary) is used to compute the object translation.

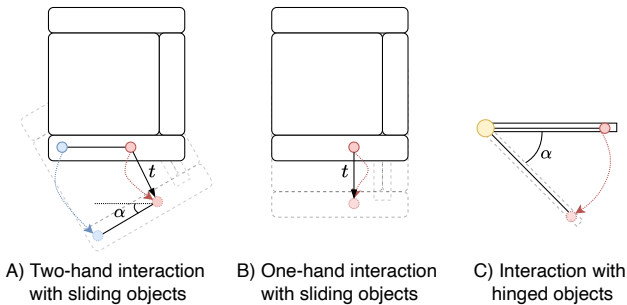


Figure 7: **Obtaining object trajectory from hand interactions.** Colored dashed lines denote hand trajectories, α is the inferred rotation angle, t is the inferred object translation vector.

B) One-hand interaction for sliding objects. When only one hand is available, it is not possible to recover the rotation of the object without a further knowledge of the object friction with the ground. In this case, we just translate the object, driven by the hand joint movement, without modifying its rotation.

C) Interaction with hinged objects. When the object movement is constrained by a hinge (*e.g.*, doors), we consider the vector that connects the hinge with the contact point on the hand. Then, we track the angle shift of this vector and rotate the door by the same amount. In the case of two hands interacting at the same time, their trajectories are averaged. We report in Supplementary more implementation details.

4. Experiments

We now show that iReplica can track scene changes from egocentric sensors, obtain visually plausible correction of human-object localization, and predict accurate contacts for interaction synthesis and object motion estimation.

4.1. Datasets

As we introduce a completely new task and method, there is a lack of appropriate datasets, baselines, and evaluation metrics. Thus we captured and annotated two new datasets: **EgoHOI** for qualitative and quantitative evaluation of egocentric human-object capture and **H-contact** for training the contact prediction model part of iReplica. We will publicly release the datasets and our annotation tool.

Egocentric Human-Object Interactions (EgoHOI) is a dataset of humans performing everyday interactions with objects in real scenes recorded with wearable sensors. The sensors are placed directly on the human to allow for large recording volumes not restricted by external camera placement. The wearable setup consists of the IMU-based motion-capturing suit Xsens Awinda [41], allowing us to obtain human pose sequences, and a head-mounted RGB camera for visual localization of the subject in the scene. Each recording location has been scanned and added to our dataset in a form of *interactive scene*. Interactive scene consists of a 3D scan of the scene, segmented objects and their degrees of freedom. EgoHOI contains 4 subjects interacting with 9 objects (tables, doors, sofas, a chair, and a metal box) in 7 interactive environments for a total of 54k frames (15 minutes). We also recorded RGBD data from external multi-camera setup to measure reconstruction accuracy; we report details and results in supplementary.

H-contact is a dataset of human-object interactions, designed to serve as a training set for our contact predictor. We collected 30 minutes of recordings divided into 3 uninterrupted sequences, for a total of 108k frames, providing interaction for 2 subjects and 3 objects. We generated validation and test subsets with 5% of the data each. We captured and annotated more than 150 human-object interactions, whose lengths range from 3 to 15 seconds. To obtain ground-truth contact classification per hand and per frame, we built a GUI-based annotation tool for this task. Based on synchronized reference RGB images of an external camera, we asked annotators to define the contact classifications.

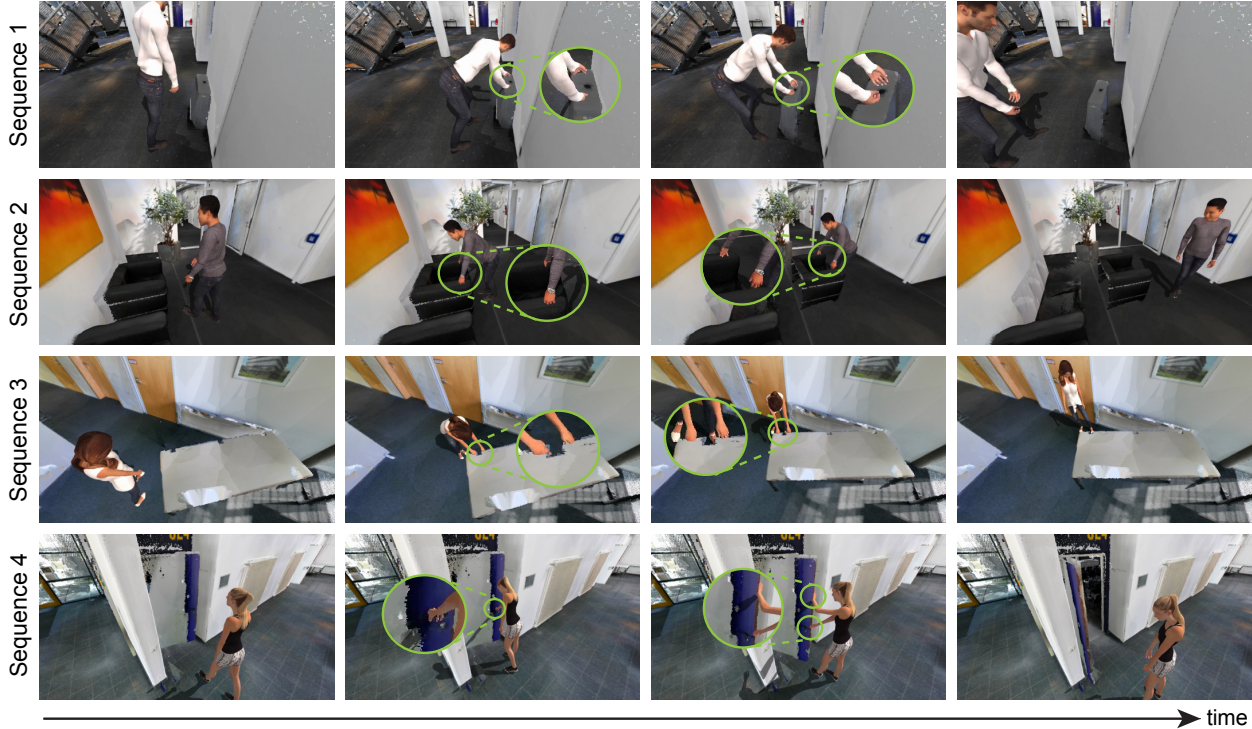


Figure 8: **Qualitative Results of iReplica.** We visualize several frames from the results of the human interacting with the object in the scene in sequential order. Mind the difference in the object position at the start and the end of the interaction (leftmost and rightmost frames). The sequences are best viewed in motion – please see the supplementary video for the animated results.

4.2. Training

The trainable part of our method is a contact predictor. Given only a human pose sequence, without surrounding scene geometry, it predicts the probability of contact with the scene for both hands.

Training details. The network is trained for 100 epochs with a batch size of 100 using the Adam optimizer [28] with learning rate of 10^{-3} and a standard binary cross-entropy loss. The resulting architecture is lightweight, with 21.9k network parameters in total and inference time of less than a second per minute of motion on an Nvidia RTX 3090 GPU. The model trained on one class of objects generalizes on the other, *i.e.*, we observed that the model trained on sofas can predict contacts with tables. However, if the motion is too different, the prediction performance drops: the model trained on door interactions does not perform well on sliding objects, and vice versa. We therefore train two separate models, one for doors and one for sofas, tables and boxes.

4.3. Baselines

Due to the novelty of the proposed human–object tracking task, no published baselines exist. To validate our finding that predicting object motion via human pose is highly effective in contrast to other paradigms, we introduce novel baselines. We briefly describe each of them below, please

see supplementary for details. We explore other strategies for object tracking: relying on GT annotations (**HPS w/ GT**), using RGB-based visual localization (**HPS w/ RGB Obj. Loc.**), or using RGB instead of IMUs for contact prediction (**iReplica w/ HOD and iReplica w/ VISOR**).

HPS. We compare to HPS [16] that localizes the human within the scene using the images of the head-mounted camera within the prescanned scene. HPS does not reason about human–object interactions and does not reconstruct object motion. Hence, it serves as a baseline to analyze the importance of including human–object reasoning when modelling interactive scenes.

HPS w/ GT combines HPS with ground-truth data to predict the object motion. It has access to the ground-truth final object pose and ground-truth start and end time of the object interaction. To obtain the object motion estimate, it linearly interpolates the object poses in the time window. Obviously, the required ground-truth data for HPS w/ GT is not available in real-world applications. This baseline is used to show that a simple linear interpolation model is not sufficient for real-world scenes. This motivates the need for more complex solutions such as ours.

HPS w/ RGB Obj. Loc. HPS only predicts the human’s pose and position. To localize the object, we use the same state-of-the-art camera localization method [46] used by

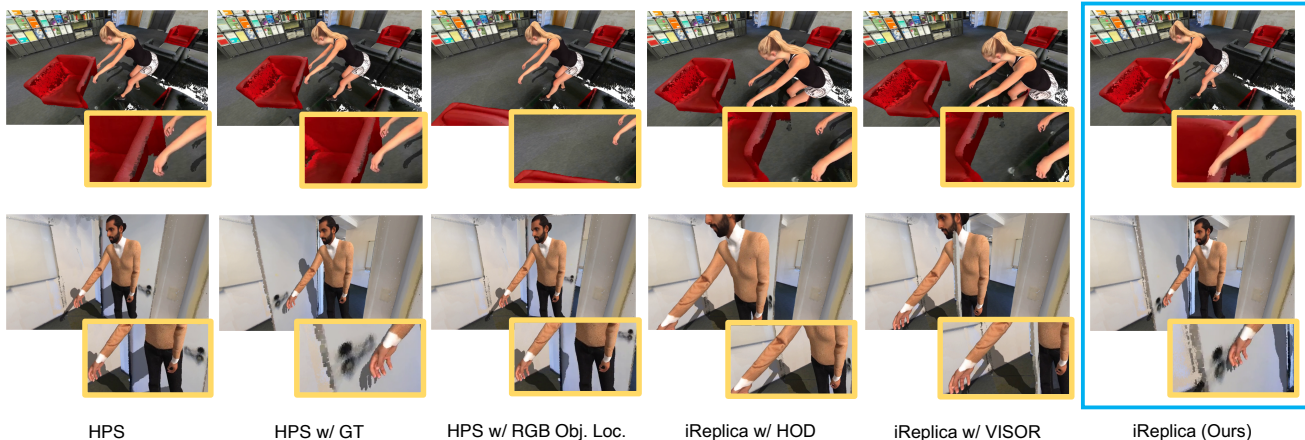


Figure 9: **Qualitative comparison.** We visually compare 6 methods: HPS, HPS w/ GT, HPS w/ RGB Obj. Loc., iReplica w/ HOD and iReplica w/ VISOR and iReplica (our method). Compared to baselines, our method, iReplica, produces realistic motion which even more realistic than the method which uses addition GT information.

HPS. Given an database of 2D images of our objects and their 3D scan in the virtual environment, [46] performs feature matching between the image of the head-mounted camera and the database. The resulting matches are then used to estimate the pose of the object w.r.t. the human. As human’s pose is known, we can obtain the global pose of the object this way. To simplify the matching process, this baseline uses GT object segmentations of the objects of interest and focuses solely on the corresponding image regions.

iReplica w/ HOD and iReplica w/ VISOR. Our approach predicts human-object contacts solely based on human pose information. Alternatively, the head-mounted RGB camera can be used to make these predictions. To compare against such baselines, we use two state-of-the-art, pre-trained, RGB-based hand-contact understanding methods: **HOD** [50] and **VISOR** [11] both predict 2D hand and object locations, and contact probabilities per hand. We use the contact probabilities as a drop-in replacement for our proposed contact predictor in iReplica, while keeping the rest of the method fixed.

4.4. Results

Qualitative results. Fig. 8 shows our results for sample frames from interactions in multiple scenes. Videos are included in the supplementary and we urge the reader to look at them as interactions are best judged in motion. Our results show that egocentric motion data alone is sufficient to localize the human in the scene, model the interaction between the human and objects, and update the scene accordingly. Our contact predictor allows iReplica to estimate object tracking only based on human pose. *E.g.*, doors in the virtual scene can be opened or objects (sofas, boxes, tables) can be displaced. Inaccuracies in human localization from the HPS are corrected plausibly as iReplica ensures that the

human and the interacted object are close to each other.

Qualitative comparisons to baselines. Fig. 9 visually compares iReplica to our baselines by showing individual frames from some of the interactions. The interactions are best viewed in the supplementary video.

HPS does not track scene changes and thus obtains unrealistic motions. For example, the door opening is not tracked and the subject passes through a closed door (Fig. 9, door). Or an object is dragged by the subject, but the object stands still, although the subject’s dragging motion is visible (Fig. 9, sofa). *HPS w/ GT* linearly interpolates object motion given ground-truth object start and end pose and timing. Human-object interaction is not visually plausible, due to a large mismatch between the motion state of the object and the subject. This illustrates the difficulty of the proposed problem: natural motion in human-object interaction is highly non-linear, making linear motion approximation infeasible. *HPS w/ Obj. Loc.* fails to detect the accurate object position during the interaction, resulting in completely misaligned results, to the point that it fails to localize the object at all (*e.g.*, Tab. 2, Box). *iReplica w/ HOD* and *iReplica w/ VISOR* both suffer from false negatives, resulting in a sudden contact loss in the middle of the interaction, leading to the object stopping midway while the subject continues to move. *iReplica* results show subjects’ hands in contact with the interaction objects during the whole interaction—a key aspect of visual plausibility not achieved by the baselines. The object trajectory is adapted according to the subjects. No offset between human and object is visible. This shows iReplica’s correction of the human trajectory based on the human-object interaction.

Reconstruction quality compared to real scenes. In this section, we quantitatively validate iReplica object and human localization results in terms of the reconstruction qual-

ity with respect to the original scene. Specifically, we measure deviations from the virtual replica to the real scene using the EgoHOI dataset. Tab. 1 shows the object localization accuracy in the end of the interaction, where the GT object pose is known. iReplica improves the results of our baselines drastically on average (col. *All*). All object types (door, sofa, table, and box) can be localized with a distance below 10 cm and an orientation error below 13 degrees.

Visual plausibility. We aim to measure the visual plausibility of iReplica results compared to the baselines. One key factor of the plausibility of interactions is that the human needs to be in contact with the object. To validate this, we measure the minimal distance from the object to the interacting hand, see Tab. 2. iReplica detects interactions and contacts at a distance below 3 cm. Keeping track of contacts and using them for attaching the object and the human motion creates the lowest human-object distances — a necessary condition for visually plausible interaction. This can be seen qualitatively in the videos.

Contact prediction accuracy. We benchmark the accuracy of iReplica contact prediction in isolation in Tab. 3. It is compared to our two RGB contact prediction baselines HOD [50] and VISOR [11]. We treat the net predictions as probabilities in a binary classification task and compute 4 metrics: Average Precision (AP), Precision, Recall and Accuracy on the binarization threshold of 0.5. Metrics are computed on the test subset of H-contact for two types of motions considered in the paper. Our contact prediction, solely based on the 3D human pose, significantly outperforms the RGB-based reasoning. This is one of our key findings: 3D human pose in isolation is a highly informative indicator of interaction contacts. This might be surprising as the RGB input from the head-mounted camera might show the actual interaction, whereas human pose lacks scene and object information. However, we found that subjects often do not directly look at the interaction and that interactions get out of view (*e.g.*, when opening a door subjects tend to not look at the handle). We hypothesize that human pose is useful due to it carrying 3D information and providing a good abstraction for generalization.

5. Discussion and Conclusion

Limitations and future work. Our work takes an important first step towards reconstructing human-object interactions in 3D scenes from wearable sensors, paving the way for affordable immersive experiences in AR/VR applications. However, we see that several challenges are still open and we look forward to future contributions by the community that may address some of them. For example, we only considered pre-scanned scenes and known interactive objects, but future advances in spatial AI technology could enable the online reconstruction of interactive envi-

Error ↓	Method	Door	Sofa	Table	Box	All
Distance (in cm)	HPS	79.27	69.54	25.31	41.92	60.81
	HPS w/ RGB Obj. Loc.	28.66	1684.06	119.59	—	597.83
	iReplica w/ HOD [50]	57.50	55.78	1.62	3.33	38.58
	iReplica w/ VISOR [11]	43.40	66.74	5.98	11.31	39.59
	iReplica (Ours)	9.97	6.66	0.90	7.09	6.88
Angle (in °)	HPS	109.19	23.53	12.16	3.76	46.89
	HPS w/ RGB Obj. Loc.	34.36	118.02	60.08	—	61.43
	iReplica w/ HOD [50]	75.74	7.74	0.78	2.71	28.41
	iReplica w/ VISOR [11]	56.64	17.36	2.87	12.78	27.27
	iReplica (Ours)	12.94	5.83	0.43	4.81	7.13

Table 1: **Object localization accuracy.** Distance (in cm) and angle (in °) between object center at the end of the interaction in the GT pose and object center in the pose predicted by the algorithm.

Method	Door	Sofa	Table	Box	All
HPS	46.00	38.32	26.35	6.64	33.61
HPS w/ GT	17.28	6.90	7.55	6.74	10.44
HPS w/ RGB Obj. Loc.	65.26	724.63	136.27	—	287.12
iReplica w/ HOD [50]	48.42	35.96	13.31	5.52	31.26
iReplica w/ VISOR [11]	33.76	51.14	13.39	3.84	31.17
iReplica (Ours)	2.83	1.46	3.49	5.49	2.93

Table 2: **Visual plausibility of human-object interaction.** Minimal distance between the object and the contacting hand (in cm) over the interaction time interval.

Predictor net / Motion	AP ↑	Precision@0.5 ↑	Recall@0.5 ↑	Accuracy@0.5 ↑
HOD [50] / Hinged	0.040	0.223	0.809	0.379
VISOR [11] / Hinged	0.200	0.101	0.033	0.753
Ours / Hinged	0.915	0.939	0.952	0.975
HOD [50] / Sliding	0.062	0.364	0.830	0.412
VISOR [11] / Sliding	0.329	0.512	0.092	0.639
Ours / Sliding	0.978	0.960	0.920	0.958

Table 3: **Contact prediction performance.** Metrics obtained on our test set split for two types of motions.

ronments. It would also be interesting to automatically discover the degrees of freedom of objects through interaction, and extending iReplica for other object classes than sliding and hinged ones (*e.g.*, 6DoF, non-rigid deformations). Another avenue of extensions could be to improve the visual quality of the contacts using hand grasp generation methods [24, 73].

Conclusion. We have introduced a challenging novel problem of simultaneously localizing a human and tracking an object in a 3D scene from wearable sensors alone. To tackle this so far unexplored problem, we gathered new datasets, established experimental protocols, designed baselines and introduced our novel approach called iReplica. Our extensive experiments have shown that human cues are sufficient for reliably estimating the motion of several types of everyday objects. Importantly, we found that the IMU-based human-object contact predictor of iReplica — without any knowledge about the scene — outperforms RGB-based alternatives. These findings enabled us to build the first system to capture human-object interaction from wearable sen-

sors alone, opening up many possibilities for developing flexible capturing solutions that can be deployed in large scenes and are not limited to the volumes covered by external cameras. By publicly releasing our code, models and data, we hope to inspire further research in this area.

Acknowledgments: Special thanks to RVH team members, and reviewers, their feedback helped improve the manuscript. This work is supported by the Deutsche Forschungsgemeinschaft (DFG, German Research Foundation) - 409792180 (Emmy Noether Programme, project: Real Virtual Humans), German Federal Ministry of Education and Research (BMBF): Tübingen AI Center, FKZ: 01IS18039A and the Czech Science Foundation (GA ĀR) EXPRO (grant no. 23-07973X). Gerard Pons-Moll is a member of the Machine Learning Cluster of Excellence, EXC number 2064/1 - Project number 390727645. Julian Chibane is a fellow of the Meta Research PhD Fellowship Program - area: AR/VR Human Understanding. Riccardo Marin is supported by an Alexander von Humboldt Foundation Research Fellowship.

References

- [1] *Autodesk FBX Software Developer Kit*, accessed March 11, 2022. <https://www.autodesk.com/developer-network/platform-technologies/fbx-sdk-2020-0>. 12
- [2] *Microsoft Azure Kinect*, accessed March 11, 2022. https://en.wikipedia.org/wiki/Azure_Kinect. 15
- [3] Bharat Lal Bhatnagar, Suriya Singh, Chetan Arora, and C.V. Jawahar. Unsupervised learning of deep feature representation for clustering egocentric actions. In *Proceedings of the Twenty-Sixth International Joint Conference on Artificial Intelligence, IJCAI-17*, pages 1447–1453, 2017. 2
- [4] Bharat Lal Bhatnagar, Xianghui Xie, Ilya A Petrov, Cristian Sminchisescu, Christian Theobalt, and Gerard Pons-Moll. Behave: Dataset and method for tracking human object interactions. In *Proceedings of the IEEE/CVF Conference on Computer Vision and Pattern Recognition*, pages 15935–15946, 2022. 2, 4
- [5] Eric Brachmann, Martin Humenberger, Carsten Rother, and Torsten Sattler. On the limits of pseudo ground truth in visual camera re-localisation. In *ICCV*, 2021. 3
- [6] Eric Brachmann and Carsten Rother. Learning Less is More - 6D Camera Localization via 3D Surface Regression. In *CVPR*, 2018. 3
- [7] Eric Brachmann and Carsten Rother. Visual camera re-localization from RGB and RGB-D images using DSAC. *arXiv:2002.12324*, 2020. 3
- [8] G. Bradski. The OpenCV Library. *Dr. Dobb’s Journal of Software Tools*, 2000. 12
- [9] Congqi Cao, Yifan Zhang, Yi Wu, Hanqing Lu, and Jian Cheng. Egocentric gesture recognition using recurrent 3d convolutional neural networks with spatiotemporal transformer modules. *2017 IEEE International Conference on Computer Vision (ICCV)*, 2017. 2
- [10] Tommaso Cavallari, Stuart Golodetz, Nicholas A. Lord, Julien Valentin, Victor A. Prisacariu, Luigi Di Stefano, and Philip H. S. Torr. Real-time rgb-d camera pose estimation in novel scenes using a relocalisation cascade. *IEEE Transactions on Pattern Analysis and Machine Intelligence (TPAMI)*, 2019. 3
- [11] Ahmad Darkhalil, Dandan Shan, Bin Zhu, Jian Ma, Amlan Kar, Richard Higgins, Sanja Fidler, David Fouhey, and Dima Damen. Epic-kitchens visor benchmark: Video segmentations and object relations. In *Proceedings of the Neural Information Processing Systems (NeurIPS) Track on Datasets and Benchmarks*, 2022. 7, 8, 15
- [12] Siyan Dong, Qingnan Fan, He Wang, Ji Shi, Li Yi, Thomas Funkhouser, Baoquan Chen, and Leonidas J Guibas. Robust neural routing through space partitions for camera relocalization in dynamic indoor environments. In *Proceedings of the IEEE/CVF Conference on Computer Vision and Pattern Recognition*, pages 8544–8554, 2021. 3
- [13] Bardia Doosti, Shujon Naha, Majid Mirbagheri, and David J Crandall. Hope-net: A graph-based model for hand-object pose estimation. In *Proceedings of the IEEE/CVF Conference on Computer Vision and Pattern Recognition*, pages 6608–6617, 2020. 2
- [14] Alireza Fathi, Ali Farhadi, and James M Rehg. Understanding egocentric activities. In *2011 international conference on computer vision*, pages 407–414. IEEE, 2011. 2
- [15] Rıza Alp Güler, Natalia Neverova, and Iasonas Kokkinos. Densepose: Dense human pose estimation in the wild. In *Proceedings of the IEEE conference on computer vision and pattern recognition*, pages 7297–7306, 2018. 1
- [16] Vladimir Guzov, Aymen Mir, Torsten Sattler, and Gerard Pons-Moll. Human positioning system (hps): 3d human pose estimation and self-localization in large scenes from body-mounted sensors. In *Proceedings of the IEEE/CVF Conference on Computer Vision and Pattern Recognition*, pages 4318–4329, 2021. 2, 3, 6, 13, 15
- [17] Mohamed Hassan, Duygu Ceylan, Ruben Villegas, Jun Saito, Jimei Yang, Yi Zhou, and Michael J Black. Stochastic scene-aware motion prediction. In *Proceedings of the IEEE/CVF International Conference on Computer Vision*, pages 11374–11384, 2021. 2
- [18] Mohamed Hassan, Vasileios Choutas, Dimitrios Tzionas, and Michael J. Black. Resolving 3D human pose ambiguities with 3D scene constraints. In *International Conference on Computer Vision*, pages 2282–2292, Oct. 2019. 2
- [19] Yinghao Huang, Omid Taheri, Michael J Black, and Dimitrios Tzionas. Intercap: Joint markerless 3d tracking of humans and objects in interaction. In *Pattern Recognition: 44th DAGM German Conference, DAGM GCPR 2022, Konstanz, Germany, September 27–30, 2022, Proceedings*, pages 281–299. Springer, 2022. 2
- [20] A. Irschara, C. Zach, J.-M. Frahm, and H. Bischof. From Structure-from-Motion Point Clouds to Fast Location Recognition. In *CVPR*, 2009. 3
- [21] Karim Isakov, Egor Burkov, Victor Lempitsky, and Yury Malkov. Learnable triangulation of human pose. In *Proceedings of the IEEE/CVF international conference on computer vision*, pages 7718–7727, 2019. 1
- [22] Ara Jafarzadeh, Manuel López Antequera, Pau Gargallo, Yubin Kuang, Carl Toft, Fredrik Kahl, and Torsten Sattler.

- Crowddriven: A new challenging dataset for outdoor visual localization. In *ICCV*, 2021. 3
- [23] Hao Jiang and Kristen Grauman. Seeing invisible poses: Estimating 3d body pose from egocentric video. In *2017 IEEE Conference on Computer Vision and Pattern Recognition (CVPR)*, pages 3501–3509. IEEE, 2017. 3
- [24] Hanwen Jiang, Shaowei Liu, Jiashun Wang, and Xiaolong Wang. Hand-object contact consistency reasoning for human grasps generation. In *Proceedings of the IEEE/CVF International Conference on Computer Vision*, pages 11107–11116, 2021. 8
- [25] Hanbyul Joo, Tomas Simon, and Yaser Sheikh. Total capture: A 3d deformation model for tracking faces, hands, and bodies. In *IEEE Conf. on Computer Vision and Pattern Recognition*, pages 8320–8329, 2018. 1
- [26] Angjoo Kanazawa, Michael J. Black, David W. Jacobs, and Jitendra Malik. End-to-end recovery of human shape and pose. In *IEEE Conf. on Computer Vision and Pattern Recognition*, 2018. 1
- [27] Diederik P Kingma and Jimmy Ba. Adam: A method for stochastic optimization. *arXiv preprint arXiv:1412.6980*, 2014. 14
- [28] Diederik P. Kingma and Jimmy Ba. Adam: A method for stochastic optimization. In Yoshua Bengio and Yann LeCun, editors, *3rd International Conference on Learning Representations, ICLR 2015, San Diego, CA, USA, May 7-9, 2015, Conference Track Proceedings*, 2015. 6
- [29] Alexander Kirillov, Yuxin Wu, Kaiming He, and Ross Girshick. Pointrend: Image segmentation as rendering. In *Proceedings of the IEEE/CVF conference on computer vision and pattern recognition*, pages 9799–9808, 2020. 15
- [30] Muhammed Kocabas, Nikos Athanasiou, and Michael J Black. Vibe: Video inference for human body pose and shape estimation. In *Proceedings of the IEEE/CVF conference on computer vision and pattern recognition*, pages 5253–5263, 2020. 1
- [31] Taein Kwon, Bugra Tekin, Jan Stuhmer, Federica Bogo, and Marc Pollefeys. H2o: Two hands manipulating objects for first person interaction recognition. *arXiv preprint arXiv:2104.11181*, 2021. 2
- [32] Yunpeng Li, Noag Snavely, Dan P. Huttenlocher, and Pascal Fua. Worldwide Pose Estimation Using 3D Point Clouds. In *ECCV*, 2012. 3
- [33] Miao Liu, Lingni Ma, Kiran Somasundaram, Yin Li, Kristen Grauman, James M Rehg, and Chao Li. Egocentric activity recognition and localization on a 3d map. In *European Conference on Computer Vision*, pages 621–638. Springer, 2022. 3
- [34] Shaowei Liu, Hanwen Jiang, Jiarui Xu, Sifei Liu, and Xiaolong Wang. Semi-supervised 3d hand-object poses estimation with interactions in time. In *Proceedings of the IEEE/CVF Conference on Computer Vision and Pattern Recognition*, pages 14687–14697, 2021. 2
- [35] Matthew Loper, Naureen Mahmood, Javier Romero, Gerard Pons-Moll, and Michael J Black. SMPL: A skinned multi-person linear model. *ACM Transactions on Graphics*, 2015. 12
- [36] Zhengyi Luo, Shun Iwase, Ye Yuan, and Kris Kitani. Embodied scene-aware human pose estimation. *arXiv preprint arXiv:2206.09106*, 2022. 1, 2
- [37] Simon Lynen, Bernhard Zeisl, Dror Aiger, Michael Bosse, Joel Hesch, Marc Pollefeys, Roland Siegwart, and Torsten Sattler. Large-scale, real-time visual-inertial localization revisited. *The International Journal of Robotics Research*, 39(9):1061–1084, 2020. 3
- [38] Minghuang Ma, Haoqi Fan, and Kris M. Kitani. Going deeper into first-person activity recognition. *2016 IEEE Conference on Computer Vision and Pattern Recognition (CVPR)*, pages 1894–1903, 2016. 2
- [39] Markus Oberweger, Paul Wohlhart, and Vincent Lepetit. Generalized feedback loop for joint hand-object pose estimation. *IEEE transactions on pattern analysis and machine intelligence*, 42(8):1898–1912, 2019. 2
- [40] Adam Paszke, Sam Gross, Francisco Massa, Adam Lerer, James Bradbury, Gregory Chanan, Trevor Killeen, Zeming Lin, Natalia Gimelshein, Luca Antiga, Alban Desmaison, Andreas Kopf, Edward Yang, Zachary DeVito, Martin Raison, Alykhan Tejani, Sasank Chilamkurthy, Benoit Steiner, Lu Fang, Junjie Bai, and Soumith Chintala. Pytorch: An imperative style, high-performance deep learning library. In H. Wallach, H. Larochelle, A. Beygelzimer, F. d'Alché-Buc, E. Fox, and R. Garnett, editors, *Advances in Neural Information Processing Systems 32*, pages 8024–8035. Curran Associates, Inc., 2019. 14
- [41] Monique Paulich, Martin Schepers, Nina Rudigkeit, and G. Bellusci. *Xsens MTw Awinda: Miniature Wireless Inertial-Magnetic Motion Tracker for Highly Accurate 3D Kinematic Applications*, 05 2018. 3, 5, 12
- [42] Georgios Pavlakos, Luyang Zhu, Xiaowei Zhou, and Kostas Daniilidis. Learning to estimate 3D human pose and shape from a single color image. In *Proceedings of the IEEE Conference on Computer Vision and Pattern Recognition*, 2018. 1
- [43] Helge Rhodin, Christian Richardt, Dan Casas, Eldar Insafutdinov, Mohammad Shafiei, Hans-Peter Seidel, Bernt Schiele, and Christian Theobalt. Egocap: egocentric marker-less motion capture with two fisheye cameras. *ACM Transactions on Graphics (TOG)*, 35(6):162, 2016. 2
- [44] Grégory Rogez, James S Supancic, and Deva Ramanan. First-person pose recognition using egocentric workspaces. In *Proceedings of the IEEE conference on computer vision and pattern recognition*, pages 4325–4333, 2015. 2
- [45] Javier Romero, Dimitrios Tzionas, and Michael J. Black. Embodied hands: Modeling and capturing hands and bodies together. *ACM Transactions on Graphics, (Proc. SIGGRAPH Asia)*, 36(6), Nov. 2017. 12
- [46] Paul-Edouard Sarlin, Cesar Cadena, Roland Siegwart, and Marcin Dymczyk. From coarse to fine: Robust hierarchical localization at large scale. In *Proceedings of the IEEE Conference on Computer Vision and Pattern Recognition*, pages 12716–12725, 2019. 3, 6, 7, 12, 15
- [47] Paul-Edouard Sarlin, Daniel DeTone, Tomasz Malisiewicz, and Andrew Rabinovich. SuperGlue: Learning Feature Matching with Graph Neural Networks. In *CVPR*, 2020. 3

- [48] Torsten Sattler, Bastian Leibe, and Leif Kobbelt. Efficient & Effective Prioritized Matching for Large-Scale Image-Based Localization. *PAMI*, 2017. 3
- [49] J. L. Schönberger, M. Pollefeys, A. Geiger, and T. Sattler. Semantic Visual Localization. In *CVPR*, 2018. 3
- [50] Dandan Shan, Jiaqi Geng, Michelle Shu, and David F Fouhey. Understanding human hands in contact at internet scale. In *Proceedings of the IEEE/CVF conference on computer vision and pattern recognition*, pages 9869–9878, 2020. 7, 8, 15
- [51] Ken Shoemake. Animating rotation with quaternion curves. In *Proceedings of the 12th annual conference on Computer graphics and interactive techniques*, pages 245–254, 1985. 14
- [52] Jamie Shotton, Ben Glocker, Christopher Zach, Shahram Izadi, Antonio Criminisi, and Andrew Fitzgibbon. Scene Coordinate Regression Forests for Camera Relocalization in RGB-D Images. In *2017 IEEE Conference on Computer Vision and Pattern Recognition (CVPR)*, 2013. 3
- [53] Konstantin Sofiiuk, Iliia Petrov, Olga Barinova, and Anton Konushin. f-brs: Rethinking backpropagating refinement for interactive segmentation. In *Proceedings of the IEEE/CVF Conference on Computer Vision and Pattern Recognition*, pages 8623–8632, 2020. 15
- [54] Sebastian Starke, He Zhang, Taku Komura, and Jun Saito. Neural state machine for character-scene interactions. *ACM Trans. Graph.*, 38(6):209–1, 2019. 2
- [55] Omid Taheri, Vasileios Choutas, Michael J Black, and Dimitrios Tzionas. Goal: Generating 4d whole-body motion for hand-object grasping. In *Proceedings of the IEEE/CVF Conference on Computer Vision and Pattern Recognition*, pages 13263–13273, 2022. 2
- [56] Omid Taheri, Nima Ghorbani, Michael J Black, and Dimitrios Tzionas. Grab: A dataset of whole-body human grasping of objects. In *Computer Vision–ECCV 2020: 16th European Conference, Glasgow, UK, August 23–28, 2020, Proceedings, Part IV 16*, pages 581–600. Springer, 2020. 2, 4
- [57] Bugra Tekin, Federica Bogo, and Marc Pollefeys. H+ o: Unified egocentric recognition of 3d hand-object poses and interactions. In *Proceedings of the IEEE/CVF conference on computer vision and pattern recognition*, pages 4511–4520, 2019. 2
- [58] Carl Toft, Will Maddern, Akihiko Torii, Lars Hammarstrand, Erik Stenborg, Daniel Safari, Masatoshi Okutomi, Marc Pollefeys, Josef Sivic, Tomas Pajdla, Fredrik Kahl, and Torsten Sattler. Long-Term Visual Localization Revisited. *TPAMI*, pages 1–1, 2020. 3
- [59] Denis Tome, Thiemo Alldeick, Patrick Peluse, Gerard Pons-Moll, Lourdes Agapito, Hernan Badino, and Fernando de la Torre. Selfpose: 3d egocentric pose estimation from a headset mounted camera. *IEEE Transactions on Pattern Analysis and Machine Intelligence*, Oct 2020. 2
- [60] Ashish Vaswani, Noam Shazeer, Niki Parmar, Jakob Uszkoreit, Llion Jones, Aidan N Gomez, Łukasz Kaiser, and Illia Polosukhin. Attention is all you need. *Advances in neural information processing systems*, 30, 2017. 4
- [61] Johanna Wald, Torsten Sattler, Stuart Golodetz, Tommaso Cavallari, and Federico Tombari. Beyond controlled environments: 3d camera re-localization in changing indoor scenes. In *European Conference on Computer Vision*, pages 467–487. Springer, 2020. 3
- [62] Zhenzhen Weng and Serena Yeung. Holistic 3d human and scene mesh estimation from single view images. In *Proceedings of the IEEE/CVF Conference on Computer Vision and Pattern Recognition*, pages 334–343, 2021. 2
- [63] Yu-Shiang Wong, Changjian Li, Matthias Niessner, and Niloy J. Mitra. Rigidfusion: Rgb-d scene reconstruction with rigidly-moving objects. *Computer Graphics Forum*, 40(2), 2021. 2
- [64] Weipeng Xu, Avishek Chatterjee, Michael Zollhoefer, Helge Rhodin, Pascal Fua, Hans-Peter Seidel, and Christian Theobalt. Mo²Cap²: Real-time mobile 3d motion capture with a cap-mounted fisheye camera. *IEEE Transactions on Visualization and Computer Graphics*, pages 1–1, 2019. 2
- [65] Xiang Xu, Hanbyul Joo, Greg Mori, and Manolis Savva. D3d-hoi: Dynamic 3d human-object interactions from videos. *arXiv preprint arXiv:2108.08420*, 2021. 2
- [66] H. Yonemoto, K. Murasaki, T. Osawa, K. Sudo, J. Shimamura, and Y. Taniguchi. Egocentric articulated pose tracking for action recognition. In *International Conference on Machine Vision Applications (MVA)*, 2015. 2
- [67] Ye Yuan and Kris Kitani. 3d ego-pose estimation via imitation learning. In *Proceedings of the European Conference on Computer Vision (ECCV)*, pages 735–750, 2018. 3
- [68] Ye Yuan and Kris Kitani. Ego-pose estimation and forecasting as real-time pd control. In *The IEEE International Conference on Computer Vision (ICCV)*, October 2019. 3
- [69] Jason Y. Zhang, Sam Pepose, Hanbyul Joo, Deva Ramanan, Jitendra Malik, and Angjoo Kanazawa. Perceiving 3d human-object spatial arrangements from a single image in the wild. In *European Conference on Computer Vision (ECCV)*, 2020. 2
- [70] Siwei Zhang, Qianli Ma, Yan Zhang, Zhiyin Qian, Taein Kwon, Marc Pollefeys, Federica Bogo, and Siyu Tang. Ego-body: Human body shape and motion of interacting people from head-mounted devices. In *Computer Vision–ECCV 2022: 17th European Conference, Tel Aviv, Israel, October 23–27, 2022, Proceedings, Part VI*, pages 180–200. Springer, 2022. 3
- [71] Siwei Zhang, Yan Zhang, Federica Bogo, Marc Pollefeys, and Siyu Tang. Learning motion priors for 4d human body capture in 3d scenes. In *Proceedings of the IEEE/CVF International Conference on Computer Vision*, pages 11343–11353, 2021. 1, 2
- [72] Xiaohan Zhang, Bharat Lal Bhatnagar, Sebastian Starke, Vladimir Guzov, and Gerard Pons-Moll. Couch: Towards controllable human-chair interactions. In *European Conference on Computer Vision (ECCV)*. Springer, October 2022. 2
- [73] Keyang Zhou, Bharat Lal Bhatnagar, Jan Eric Lenssen, and Gerard Pons-Moll. Toch: Spatio-temporal object-to-hand correspondence for motion refinement. In *European Conference on Computer Vision (ECCV)*. Springer, October 2022. 8

SUPPLEMENTARY MATERIALS

Interaction Replica: Tracking human–object interaction and scene changes from human motion

Abstract

In this document we present additional details about driving the object using contacts, correcting the human trajectory and handling additional hand information. We also describe our capturing setup and provide further results not included in the main manuscript due to space limitations.

6. Human POSEitioning System (HPS)

For completeness, we briefly introduce HPS, the system we use in our pipeline to provide initial human poses.

The HPS pipeline produces poses for the SMPL [35] model together with the global position within the 3D scan coordinate system. It uses data from the body-mounted sensors, the video from the head-mounted camera, and the 3D point cloud of the pre-scanned scene as input. The output represents the human localized in the 3D scene. HPS relies on three steps:

1) Pose estimation from XSens. From the IMU measurements, XSens uses a proprietary algorithm based on the Kalman filter and a kinematic body model, which takes physical limitations of the body into account. The system provides the human pose and translation estimation in its own coordinate frame. While these estimates can be considered accurate, the system has two main drawbacks: it accumulates errors over time, leading to significant drift, and the human dynamic is not registered within the global 3D scene, causing potential inconsistencies (*e.g.*, wall and floor penetration).

2) Head-mounted camera localization. For every camera frame, HPS provides the initial head pose estimates using a hierarchical localization algorithm [46], which operates on RGB images. Given a dataset of images with known positions in the pre-scanned scene, the algorithm establishes correspondences between those images and the camera frame, finding the position of the head camera by minimizing the reprojection loss. The camera lets HPS globally localize the human in the scene, but the raw localizations are noisy and do not ensure realistic human placement in the scene.

3) Combining IMUs and the head-mounted camera. HPS combines the two previous steps together with the

3D point cloud of the pre-scanned scene to optimize the human pose and satisfy all the previously mentioned constraints. The simultaneous optimization for the IMU-based body poses and camera localizations eliminates the noise of the camera pose predictions, and significantly decreases IMU drift at the same time, resulting in stable and accurate results.

7. Capturing Setup

We use a combination of the Xsens Awinda [41] IMU system to capture body motions and a head-mounted camera (Apple iPhone 12 or GoPro Hero 8) to capture the first-person view. The camera captures at a resolution of 1920×1440 , 30 FPS. While both cameras feature automatic stabilization, we explicitly turn it off to get a better idea of the head motion. We use OpenCV [8] to calibrate the camera intrinsics. The Xsens Awinda consists of 17 IMU sensors attached to the body with velcro straps and captures the body motion at 60 FPS.

The Xsens Awinda outputs human poses in the form of skeleton joint angles, which is not directly compatible with the SMPL [35] pose parameters format. To convert between these formats, we developed the following retargeting algorithm: we export the motion from the Xsens internal format (MVN) into the Autodesk FBX format and use the Autodesk FBX Python SDK [1] to extract the rotation of each joint as a quaternion. We convert those quaternions to the axis-angle representation used in SMPL. We map joint rotations from the FBX skeleton to the SMPL skeleton according to a manually designed mapping. Finally, we produce the SMPL pose parameter vector by concatenating the mapped axis-angle joint rotations in the right order.

8. Adding Hands Data

If fine-grained hand positions are available (*e.g.*, captured with motion capture gloves), we can modify the algorithm to consider such data. Namely, we replace the SMPL model with SMPL+H [45], which has the same template body mesh, but provides additional 30 joints (3 joints for each finger) for detailed hand pose representation. We additionally change the input of our contact prediction network to accept vectors of concatenated body pose and hand pose parameters, therefore the input becomes 61 vectors of size

$1 \times \hat{S}$, $\hat{S} = 159$, adding 90 parameters of hands pose to each input vector. No additional architecture changes are made.

9. Driving the Object Based on Contacts

In this section, we provide more details on the object motion driven by human contact, also depicted in Fig. 10.

Processing the contact intervals. To remove false negatives, we post-process the predicted sequence and fill in gaps between active contacts that are shorter than 0.5 s, which produced the best results on a validation set (see the inset table).

t	Error (cm)
0.00	13.61
0.25	8.49
0.50	7.13
1.00	8.86
2.00	8.86

We set $t = 0.5$, since it produced the smallest error among the different tested values, as reported in the table on the right. Each group of consecutive frames with active contact is considered a *contact interval*.

Degrees of freedom. We model the degrees of freedom (DOF) of the motion of each object as to avoid unrealistic motions. For example, a door can only rotate around a specific axis, and a sofa can only slide along the floor. While our model operates in a 3D scene, we present all derivations in 2D, since all the processed motion happens along the floor and any change in the direction orthogonal to the movement plane does not affect the object trajectory and will be removed.

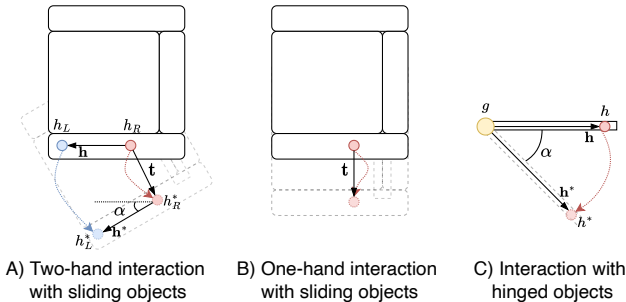


Figure 10: **Obtaining object trajectory from hand interactions (extended version of the figure from the main paper).** Colored dashed lines denote hands trajectories, α is inferred rotation angle, t is inferred object translation vector

A) Two-hands interaction with sliding objects. We consider the point cloud of an interactive object $O \in \mathbb{R}^{n \times 3}$ that can be freely moved on a two-dimensional plane. When the two hands contact the object, we denote the position of two keypoints corresponding to the middle of each hand as $h_L = (x_L, y_L)$ and $h_R = (x_R, y_R)$ for the left and the right hand, respectively, and h as the vector that connects h_R to h_L . When the human moves, we register the new positions of the hands as h_L^* and h_R^* , together with the new connecting vector h^* . Then, we compare the hand configurations to recover a translation and a rotation. Firstly, we define the

translation t as

$$t = (x_R^* - x_R, y_R^* - y_R). \quad (1)$$

Then we compute the rotation angle as

$$\alpha = \arccos \left(\frac{h h^*}{|h| |h^*|} \right). \quad (2)$$

Finally, we recover the 2D rotation matrix R^α associated with the angle. The direction of the rotation (sign of α) can be computed as a sign of a Z coordinate of the cross-product of 3D vectors with X and Y coordinates equal to X and Y coordinates in h and h^* and Z coordinate set to 0.

B) One-hand interaction with sliding objects. When only one hand h interacts with the object, without any further information about the object’s physics (e.g., its friction with the ground), it is impossible to recover the object rotation. Hence, given a new configuration h^* , we just compute the translation

$$t = (\hat{x} - x, \hat{y} - y). \quad (3)$$

C) Interaction with hinged objects. In this case, the object has a hinge positioned in $g = (x_g, y_g)$. When the contact begins at the point $h = (x_h, y_h)$, we compute the vector h that connects g to h :

$$h = (x_h - x_g, y_h - y_g). \quad (4)$$

When the human moves, we register the new position of the contact point h^* and accordingly recompute the connecting vector h^* . Then we compute the angle α between h and h^* as in Equation 2, and we recover the associated rotation matrix R^α .

After obtaining these transformations, we apply them to the first two coordinates of each point of the object O .

$$O^* = R^\alpha O + t \quad (5)$$

10. Deforming the Human Trajectory

Goal. Our method relies on a combination of data coming from the IMUs and head-mounted camera, from which we need to get the human poses. We use the HPS [16] method for this. However, the motions from HPS can give inconsistent predictions. According to [16], HPS has a body localization error around 4–16 cm, which is usually acceptable for global body positioning, but affects the result during fine-grained actions like object interaction. In our setting, we need to align the hands to the contact point predicted by our method – this is fundamental to obtaining a realistic object motion. For this, we could choose to either globally

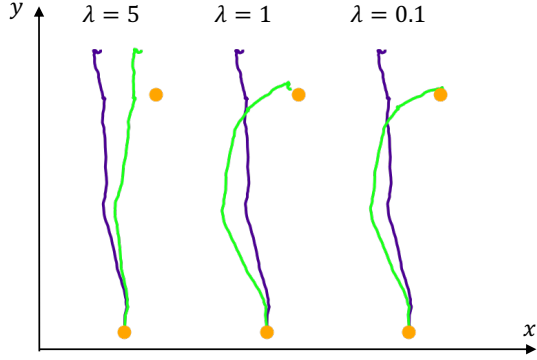


Figure 11: **Trajectory fitting with bending energy.** Bending trajectories with F_{tr} using different rigidity coefficients λ , purple marks the original trajectory, green marks the result, orange dots denote control points.

translate the trajectory to satisfy the contacts or use a special optimization method which ensures smooth adaptation to the contact points while keeping the motion trajectory as intact as possible. We describe this latter method below.

Overview. We formulate a simple optimization to correct the human pose and localization, balancing the deviation induced by the inferred point of contact and the adherence to the trajectory initially predicted by HPS. The intuition is to preserve the trajectory’s local characteristics (first and second derivatives, curvature) while satisfying constraints given by a general number of control points (in our case, the contact point at the start of the interaction). To provide a physical intuition, we consider the trajectory as a “bending tape”: it is not allowed to modify its length but can bend accordingly to a rigidity coefficient. Even though we are working with 3D trajectories, we keep the coordinates along the direction of gravity fixed (our scene coordinate system always has such an axis), hence it is sufficient to discuss the case of 2D trajectories in the following.

“Bending” energy. Given a trajectory described as a curve $\mathbf{l}(\tau) = (x(\tau), y(\tau))$, $\tau = [\tau_{\text{start}}, \tau_{\text{end}}]$, and a list of K control points $\mathbf{p} = \{\mathbf{p}_i = (x_i, y_i)\}_{i=1}^K$ (constraints) at times $\tau_{\text{start}} \leq \tau_1, \dots, \tau_K \leq \tau_{\text{end}}$, we minimize the trajectory bending energy E_{tr} and the distance to the control points as follows:

$$F_{tr}(\mathbf{l}, \mathbf{p}) = \arg \min_{\hat{\mathbf{l}}} \left(\sum_{i=1}^K (\|\hat{\mathbf{l}}(\tau_i) - \mathbf{p}_i\|_2) + \lambda E_{tr}(\hat{\mathbf{l}}, \mathbf{l}) \right), \quad (6)$$

where λ is the tape rigidity coefficient (Fig. 11, A). The bending energy penalizes deviations from the initial curve \mathbf{l}

$$E_{tr}(\hat{\mathbf{l}}, \mathbf{l}) = \int_{\tau_{\text{start}}}^{\tau_{\text{end}}} \left(\frac{d\hat{\alpha}(\tau)}{d\tau} - \frac{d\alpha(\tau)}{d\tau} \right) d\tau, \quad (7)$$

where

$$\hat{\alpha}(\tau) = \text{atan2} \left(\frac{d\hat{y}}{d\tau}, \frac{d\hat{x}}{d\tau} \right), \quad \alpha(\tau) = \text{atan2} \left(\frac{dy}{d\tau}, \frac{dx}{d\tau} \right),$$

$$\text{atan2}(y, x) = \begin{cases} \arctan\left(\frac{y}{x}\right) & \text{if } x > 0, \\ \arctan\left(\frac{y}{x}\right) + \pi & \text{if } x < 0 \text{ and } y \geq 0, \\ \arctan\left(\frac{y}{x}\right) - \pi & \text{if } x < 0 \text{ and } y < 0, \\ +\frac{\pi}{2} & \text{if } x = 0 \text{ and } y > 0, \\ -\frac{\pi}{2} & \text{if } x = 0 \text{ and } y < 0, \\ \text{undefined} & \text{if } x = 0 \text{ and } y = 0. \end{cases}$$

Here, α is the angle of the curve’s tangent vector and the energy penalizes deviations of the angle’s temporal derivative. We can interpret this as enforcing curvature preservation.

11. Implementation and Performance

We implement our algorithms in Python using the PyTorch [40] library for the contact prediction network and the bending energy optimization algorithm. For the latter, we use the Adam [27] optimizer with 1000 iterations, with the learning rate and the rigidity coefficient λ acting as hyperparameters.

The most computationally expensive part of our algorithm is the visual localization pipeline needed for HPS, requiring 8 seconds per frame on an NVIDIA Q8000 GPU, while the other steps take little additional time. Such a computationally expensive pipeline provides good localization results and supports our exploration. Note that the performance of the visual localization network itself is not the focus of our study, and we expect that more efficient alternatives can replace this algorithm in the future.

12. Baselines

In this section, we provide additional details for the baselines used in the paper.

HPS w/ GT. In this baseline, we assume that an oracle provides the ground-truth final object position, as well as the time window of the interaction. We stress that in our setting, neither of these is available at inference time, and our method does not rely on them. Then the human motion is solely estimated using HPS, and the object movement is modelled using linear interpolation for translation and spherical linear interpolation (Slerp [51]) for rotation. By inspecting the qualitative results (please refer to the attached video), we see that motion between humans and objects happens asynchronously and, therefore, unrealistically. This baseline shows that, even in the presence of further assumptions, modelling the object trajectory is non-trivial. It is clear that human motion is rarely linear, and more sophisticated techniques are required.

HPS w/ RGB Obj. Loc. In this baseline, we assume that for each frame of the head-mounted camera, we have a perfect 2D segmentation mask for the object, obtained by semi-automatic annotation using an interactive segmentation pipeline [53]. Then we use the same localization method [46] as HPS to provide a 6-DoF localization of the object w.r.t. the human. Starting from the dataset of images with the known object positions in the pre-scanned scene, the algorithm establishes correspondences between those images and frames from the head-mounted camera. The head-mounted camera is then localized by minimizing reprojection loss. Finally, the object’s location relative to the camera is recovered by matching only the 2D keypoints inside the object mask. This information is combined with the camera position to recover the location of the object in world coordinates. This baseline highlights that the camera is not reliable for localizing the object in the space. Detecting local landmarks is dramatically harmed by occlusions, head shaking, and the object missing in several frames.

iReplica w/ HOD. Given the availability of a head-mounted camera, we explore the possibility of using it to predict contacts. In this baseline, we replace our IMU-based contact predictor with HOD [50], a method trained on a large set of YouTube videos. Starting from a single RGB image, it predicts a full set of hand interaction properties: hands box, object box, and also the contact state for each hand. Except for the contact prediction part, we keep the rest of our method fixed.

The original paper [50] shows several results from an egocentric perspective, but it also mentions failure cases when hands and objects are close to each other. We confirm this by qualitative inspection, noting that the method loses contact with the object during the interaction.

iReplica w/ VISOR. Given that HOD is trained on a variety of videos which also include extrinsic views, we deploy a similar baseline but rely on an RGB method specifically trained on egocentric views. Specifically, we consider the baseline trained for the HOS challenge² on the VISOR [11] dataset. This baseline relies on PointRend [29], augmented with auxiliary detection heads to predict the contact, following the same schema of HOD [50]. As in the previous baseline, we replace our IMUs-based contact prediction, leaving other parts of the method untouched. However, also in this case, we observe missing contacts and wrong release prediction, often causing human penetration (*e.g.*, crossing the door).

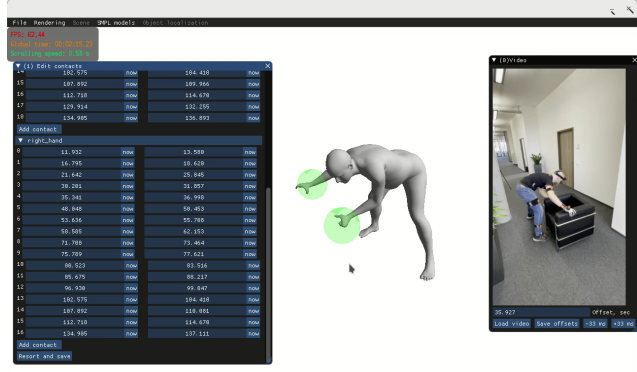


Figure 12: **Annotation tool.** The user views the RGB video frames (*right*) and annotates the start and the end of contact interaction (*left*). To help with disambiguating occlusions, the tool also shows the 3D pose (*center*) together with the annotated presence of contact for each hand (green circles).

	Human to GT $E_{body} \downarrow$	Object to GT $E_{obj} \downarrow$
HPS	9.771	22.651
iReplica (ours)	8.981	8.471

Table 4: **Human and object tracking quality w.r.t. the real scene:** Mean 3D error (in cm) between tracked and moving human/object models compared to the real scene. The scene is captured via a synchronized, multi-view RGBD video recording setup observing the interaction.

13. External Camera Evaluation

To additionally measure the human-object localization accuracy of our method, we recorded a special sequence which additionally has ground-truth data obtained via an external multi-view system of depth cameras. The experimental setup closely follows the one used in HPS [16], however we capture the full dynamic object interaction while in HPS only the human body motion and the static scene was captured.

We use 3 calibrated Azure Kinect [2] RGBD sensors. By combining the outputs of these sensors, we obtain a sequence of 3D point clouds of the scene and a subject. Each sensor outputs the depth map with a resolution of 640×576 pixels and color frames with a resolution of 2048×1536 at around 30 FPS. The Azure Kinect features built-in temporal synchronization, but to merge the output of the sensor into the scene ground truth representation, we also need to calibrate them spatially. For that we use a three-stage localization pipeline, similar to [16]: **1)** we record a special sequence with 300 frames depicting the empty scene. We localize the RGB camera in each of these frames using the same algorithm as used for the head-mounted camera and average the 300 localization results; **2)** we perform ICP between the scene 3D scan and the point cloud unpro-

²<https://github.com/epic-kitchens/VISOR-HOS>

jected from the depth map; **3**) we apply manual corrections if needed. Using the obtained positions of the sensors, the point cloud representation of the scene is formed by unprojecting depth maps from all 3 sensors to 3D. To perform the evaluation, we manually synchronize the time between the iReplica motion sequence and the aforementioned point cloud representation. For each frame of the test sequence, we separately measure object and human localization accuracy E_{obj} and E_{body} :

- E_{obj} : mean Chamfer distance from the object point cloud to ground-truth point cloud,
- E_{body} : mean Chamfer distance from the human body SMPL mesh to ground-truth point cloud.

Results are presented in Table 4. Since HPS models only humans, the large error from the object ground truth is not surprising. Although HPS and iReplica share the same camera localization principle, we observe that our iReplica improves human localization. This validates that using the detected human–object interaction to adapt the human localization trajectory helps to improve reconstruction correctness. Moreover, it drastically enhances visual plausibility, as explained in the qualitative analysis.

14. Annotation Tool

Fig. 12 is a screenshot of our annotation tool for preparing our H-contact dataset. Given a video frame (*right*) and the reconstruction (*center*), the user can annotate contacts by clicking on the interacting hands. The annotator can seek forwards and backwards in the video, and the 3D reconstruction helps to disambiguate occluded poses. On average, it takes around 2–4 seconds to annotate 1 second of video.

15. Examples from the Datasets

In Fig. 13 we report some examples from the H-contact and EgoHOI datasets. For H-contact, we provide IMU measurements, SMPL parameters, head-mounted RGB videos, contact annotations, and external camera recordings. For EgoHOI, we provide recordings from multiple RGB cameras, IMU data, as well as contact labels and GT final object positions (for evaluation purposes).

16. More Results

Fig. 14 shows further results of iReplica on the sequence, recorded to simulate a realistic and natural scenario, highlighting several features that make our method particularly compelling. iReplica does not assume a single object interaction: instead, it applies to interactive scenes where many objects can be differently re-arranged by the interaction (*e.g.*, table, chair). iReplica also works with objects with

non-linear motion in space, for example, the doors which might start and end their movement in the same place. In this case, an interpolation baseline would not provide any object dynamic, since the initial and final configurations are the same. Instead, iReplica keeps track of all the state changes of the object. iReplica allows the user to move in the space freely and interact naturally as in everyday life. We refer to the supplementary video for the animated results.

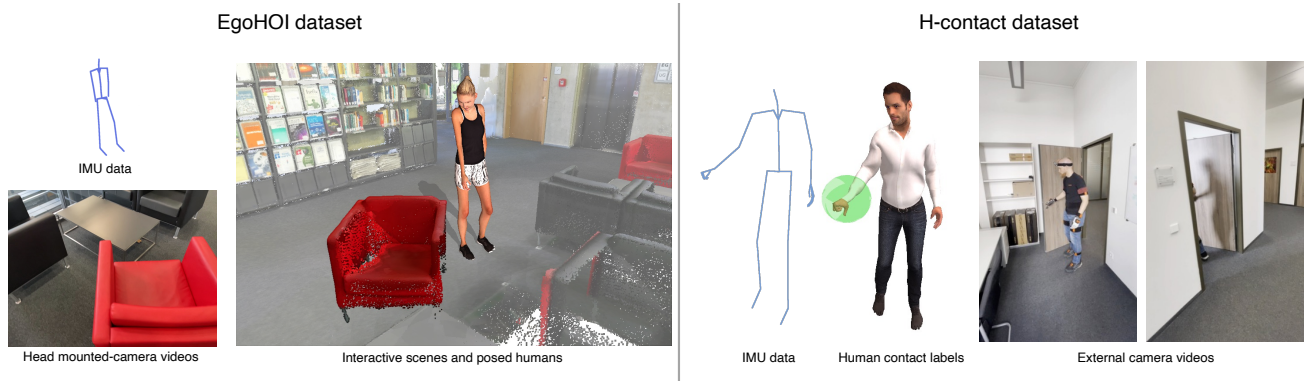


Figure 13: **EgoHOI and H-Contact examples.** For EgoHOI, we report for each timestamp the data obtained by the IMUs, the head mounted-camera frame, and the 3D posed human inside the interactive scene. For H-Contact, we provide IMUs data, contact labels for each hand, and the recording from external cameras.

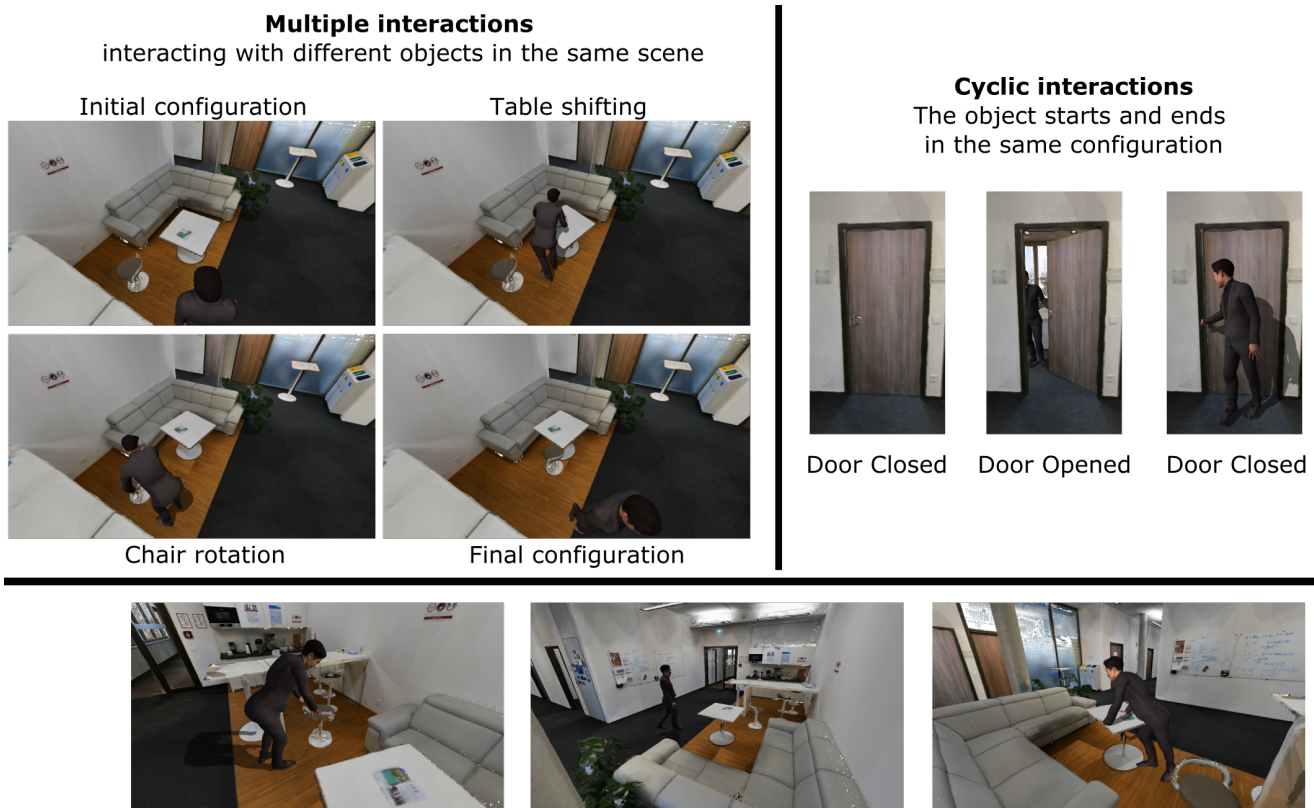


Figure 14: **iReplica Features.** iReplica handles different kinds of challenges. It can be naturally applied to interactions involving several objects (*e.g.*, arranging a table and a chair), objects that have a cyclic behavior in the scene (*e.g.*, doors that open and close several times), and general daily interactions where the user freely moves in the space (*e.g.*, walking to the kitchen, pushing a table). Please see the supplementary video for animated results.